Tunable Fano resonances and enhanced optical bistability in composites of coated cylinders due to nonlocality

Yang Huang and Lei Gao*

College of Physics, Optoelectronics and Energy of Soochow University, Collaborative Innovation Center of Suzhou Nano Science and Technology, and Jiangsu Key Laboratory of Thin Films, Suzhou 215006, China

(Received 15 May 2016; published 23 June 2016)

Theoretical studies of the optical bistability in two-dimensional nonlinear composites, where Kerr type dielectric/nonlocal metal core-shell cylinders are randomly embedded in the host medium, have been carried out. Within the quasistatic approximation, we demonstrate the tunable Fano resonances in the scattering spectra of the single core-shell cylinder based on different degrees of nonlocality in the linear case. It is found that nonlocality of the metallic shell would enhance the Fano resonance peak and the near-field strength, thus it can further boost the nonlinear response of the core-shell cylinder in both near field and far field, indicating the nonlocality-enhanced optical bistability. Furthermore, we show that nonlocality can efficiently reduce the bistable switching threshold of the nonlinear composite, and these self-tunable optical resonant scatters can be used as all-optical switches and nanomemories.

DOI: 10.1103/PhysRevB.93.235439

I. INTRODUCTION

Nanosized dielectric/metal structures have long been used as optical metamaterials to realize light manipulation [1]. Nonlinear optical effects [2] that could enable nonlinear light-matter interaction have played an important role in modern optics and provide potential applications on ultrafast optical switching, optical transistors, optical modulation, and so on [3]. Compared with single nonlinear dielectric or metal, the composite structure consisting of dielectric and metal can support surface plasma [4], which will confine and enhance the local electromagnetic fields, hence significantly boosting the nonlinear optical response. Such effects arise from coherent oscillations of conduction electrons near the surface of noble-metal structures [4,5], whose resonances are strongly dependent on the size and shape of the inclusions, as well as the dielectric medium. Recently, compact plasmonic-enhanced-nonlinear functionalities with dielectric/metal materials have been widely investigated [6–10].

Optical bistability is one remarkable feature of nonlinear effects [11,12]. It is a way of controlling light with light where a nonlinear optical systems shows two different values of the local field intensity for one input intensity [13]. This novel property can give the optical structures the function to control two distinguishing stable states with the history of the input light, which can be further employed in optoelectronics and logic elements. Along this line, one of our authors developed a self-consistent mean-field approximation in conjunction with the spectral representation method to investigate the optical bistability of nonlinear plasmonic composites [14,15]. It showed that there exists double optical bistability and optical tristability in nonlinear plasmonic composites of nonspherical nanoparticles. Most recently, we proposed the graphene wrapped nonlinear composite and achieved the optical bistability in its near fields as well as the transmission spectra [16]. Due to recent advances in the development of high-quality nanostructured systems, it is possible to engineer the field penetration inside the nanostructure to use its nonlinear response. For instance, plasmonic kinks, solitons, and domain well are reported in arrays of nonlinear plasmonic nanoparticles [17,18]. Light switching and routing in nonlinear metal-dielectric nanoantennas [19] and optical bistability in a nonlinear plasmonic nanoantenna array with reflecting surface [20] are the other demonstrations. Some researchers also proposed nonlinear plasmonic cloaks [21] and film-coupled plasmonic nanocubes [22] to realize giant all-optical scattering nanoswitches controlled by moderate pumping intensity.

On the other hand, once the dimension of the dielectric/metal structure is down to the tens-of-nanometers level, the electron-electron interactions in the dielectric response of metals should be taken into account [23]. Consequently, conventional local solution of Maxwell's equations are no longer able to describe electromagnetic properties accurately. In this regard, nonlocal theory should be adopted because of its more accurate description in comparison with local theory [24,25]. Nonlocality arises from the electron-electron interactions and leads to the spatial dispersion of metals, hence it will play a further role in the metal's surface plasmons. In fact, nonlocality was found to reduce the expected field enhancements [26–35], suggesting that nonlinear processes may also be affected. Actually, influence of surface electrons interaction on the nonlinear current in the gap of the two dimer [36] was reported. Recently, nonlocal effects on third harmonic generation in the gap nanostructure [37,38] are also studied. To the best of our knowledge, nonlocal effects on the optical bistability have not been explored yet. In this paper, we theoretically propose a two-dimensional dielectric/metal composite where Kerr dielectric core-nonlocal metallic shell cylinders are embedded in the host medium, and we show that the inclusion of nonlocal effects can dramatically alter the near-field configuration and far-field scattering signals of core-shell cylinder composite. We demonstrate that the nonlocality would lead to the tunable Fano resonances in the scattering spectra of the core-shell inclusion. It is found that the nonlocality can significantly reduce the switching threshold of the optical bistability in the near field and far field, suggesting a nonlocality enhanced nonlinear optical device.

*leigao@suda.edu.cn

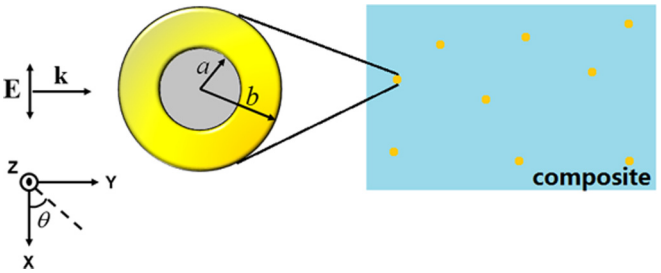

FIG. 1. Schematic diagram of the model.

II. FORMULATION

Let us first start with a linear case of two-dimensional composite, whose schematic diagram is shown in Fig. 1. We consider the external electric field $\mathbf{E} = E_0(\omega)\hat{e}_x$ lighting upon an infinitely long core-shell nanocylinder with inner radius a and outer radius b, embedded in the host medium ε_h. The shell material of the cylinder is described by a spatial dispersive dielectric function $\varepsilon(\mathbf{k},\omega)$. Since the size of the nanocylinder is much smaller than the incident wavelength here, we neglect the retardation effect. Outside the cylinder, the total electric potential, including the external and induced ones, is given by

$$V(\mathbf{r}) = -E_0 r\cos\theta + \frac{\alpha}{r}\cos\theta, \tag{1}$$

where $\mathbf{r} = (r,\theta,z)$ is the cylindrical coordinate whose origin is at the cylinder center and α is the induced line dipole polarizability. The corresponding displacement vector $\mathbf{D}$ is determined by the following relation,

$$\mathbf{D}(\mathbf{r}) = -\varepsilon_\mathrm{h}\nabla V(\mathbf{r}). \tag{2}$$

Inside the shell region, we introduce the so-called semiclassical infinite barrier (SCIB) model [39,40] to derive its electrostatic potentials. The electric field and displacement vector satisfy the electrostatic equations,

$$\begin{aligned}\nabla\cdot\mathbf{D} &= 0\\ \nabla\times\mathbf{E} &= 0\end{aligned} \tag{3}$$

with the field intensity $\mathbf{E}$ and the displacement $\mathbf{D}$ being related through the nonlocal relation in homogeneous medium,

$$\mathbf{D}(\mathbf{r}) = \int \varepsilon(\mathbf{r}-\mathbf{r}',\omega)\mathbf{E}(\mathbf{r}')d^3r'. \tag{4}$$

We then define the potential for the displacement as

$$\mathbf{D}(\mathbf{r}) = -\nabla V_\mathrm{D}(\mathbf{r}) \tag{5}$$

and introduce an infinite fictitious media as the assumption of an SCIB model. With charge sources of the appropriate symmetry located on the inner and outer interfaces, we get the Poisson-type equation to solve as

$$\nabla^2 V_\mathrm{D}(\mathbf{r}) = [A\delta(r-a) + B\delta(r-b)]\cos\theta, \tag{6}$$

where A and B are the unknown coefficients to be determined. Taking the Fourier transform of Eq. (6), we have

$$-k^2 V_\mathrm{D}(\mathbf{k}) = \int [A\delta(r-a) + B\delta(r-b)]e^{-i\mathbf{k}\cdot\mathbf{r}}\cos\theta d^2r. \tag{7}$$

Note that $e^{-i\mathbf{k}\cdot\mathbf{r}}$ can be expanded as

$$e^{-i\mathbf{k}\cdot\mathbf{r}} = \sum_{n=-\infty}^{\infty}(-i)^n J_n(kr)e^{-in(\theta-\theta_k)}, \tag{8}$$

where (k,θ_k) and (r,θ) are the cylindrical coordinates of $\mathbf{k}$ and $\mathbf{r}$, respectively, and $J_n(x)$ is the Bessel function of the first kind. Substituting Eq. (8) into Eq. (7), we yield

$$V_\mathrm{D}(\mathbf{k}) = i2\pi\frac{AaJ_1(ka) + BbJ_1(kb)}{k^2}e^{i\theta_k}. \tag{9}$$

Taking the anti-Fourier transform of Eq. (9), the potential for displacement vector in real space can be written as

$$V_\mathrm{D}(\mathbf{r}) = -\frac{1}{2}\left[A\frac{a^2}{r} + Br\right]\cos\theta. \tag{10}$$

The constitutive equation in Eq. (4) has an alternative expression as $V_D(\mathbf{k}) = \varepsilon(\mathbf{k},\omega)V(\mathbf{k})$ in $\mathbf{k}$ space, and one could yield the electric potential inside the nonlocal shell as

$$V(\mathbf{r}) = -\left[Aa\int\frac{J_1(ka)J_1(kr)}{k\varepsilon(k,\omega)}dk + Bb\int\frac{J_1(kb)J_1(kr)}{k\varepsilon(k,\omega)}dk\right]\cos\theta. \tag{11}$$

Therefore, electric potentials V_q ($q = \mathrm{c,s,h}$ denote the core, the shell, and the host medium) and displacement potentials $V_{\mathrm{D}q}$ throughout the whole space have the following general expressions,

$$\begin{aligned}
V_\mathrm{c}(r) &= -E_0 Cr\cos\theta && (r<a)\\
V_\mathrm{s}(r) &= -E_0\left[Aa\int\frac{J_1(ka)J_1(kr)}{k\varepsilon(k,\omega)}dk + Bb\int\frac{J_1(kr)J_1(kb)}{k\varepsilon(k,\omega)}dk\right]\cos\theta && (a<r<b)\\
V_\mathrm{h}(r) &= -E_0(r - D/r)\cos\theta && (r>b),
\end{aligned} \tag{12}$$

and

$$V_{\mathrm{D}s}(r) = -\frac{1}{2}E_0\left[A\frac{a^2}{r} + Br\right]\cos\theta, \tag{13}$$

where A, B, C, and D are the coefficients to be determined. We impose the boundary conditions [41] as follows

$$\begin{aligned} V_c|_{r=a} &= V_s|_{r=a} \\ V_s|_{r=b} &= V_h|_{r=b} \\ \varepsilon_c \cdot \partial_r V_c|_{r=a} &= \partial_r V_{Ds}|_{r=a} \\ \partial_r V_{Ds}|_{r=b} &= \varepsilon_h \cdot \partial_r V_h|_{r=b}, \end{aligned} \tag{14}$$

and the corresponding matrix equation for the four unknown coefficients is

$$\begin{pmatrix} a/[2f(a,a)] & a/[2f(a,b)] & -a & 0 \\ a^2/[2bf(a,b)] & b/[2f(b,b)] & 0 & 1/b \\ 1/2 & -1/2 & \varepsilon_c & 0 \\ a^2/(2b^2) & -1/2 & 0 & \varepsilon_h/b^2 \end{pmatrix} \times \begin{pmatrix} A \\ B \\ C \\ D \end{pmatrix} = \begin{pmatrix} 0 \\ b \\ 0 \\ -\varepsilon_h \end{pmatrix}, \tag{15}$$

where

$$f(x,y) = \left[2\frac{y}{x} \int \frac{J_1(kx)J_1(ky)}{k\varepsilon(k,\omega)} dk \right]^{-1}, \quad (x < y). \tag{16}$$

Solving the above equations, we have

$$\begin{aligned} A &= \frac{4f(a,a)f(a,b)f(b,b)\varepsilon_h[f(a,b)-\varepsilon_c]}{-(a/b)^2 f(a,a)f(b,b)[f(a,b)-\varepsilon_c][f(a,b)-\varepsilon_h] + f(a,b)^2[f(a,a)+\varepsilon_c][f(b,b)+\varepsilon_h]} \\ B &= \frac{4f(a,b)^2 f(b,b)\varepsilon_h[f(a,a)+\varepsilon_c]}{-(a/b)^2 f(a,a)f(b,b)[f(a,b)-\varepsilon_c][f(a,b)-\varepsilon_h] + f(a,b)^2[f(a,a)+\varepsilon_c][f(b,b)+\varepsilon_h]} \\ C &= \frac{2f(a,b)f(b,b)\varepsilon_h[f(a,a)+f(a,b)]}{-(a/b)^2 f(a,a)f(b,b)[f(a,b)-\varepsilon_c][f(a,b)-\varepsilon_h] + f(a,b)^2[f(a,a)+\varepsilon_c][f(b,b)+\varepsilon_h]} \\ D &= b^2 \frac{f(a,b)^2[f(a,a)+\varepsilon_c][f(b,b)-\varepsilon_h] - (a/b)^2 f(a,a)f(b,b)[f(a,b)-\varepsilon_c][f(a,b)+\varepsilon_h]}{-(a/b)^2 f(a,a)f(b,b)[f(a,b)-\varepsilon_c][f(a,b)-\varepsilon_h] + f(a,b)^2[f(a,a)+\varepsilon_c][f(b,b)+\varepsilon_h]}. \end{aligned} \tag{17}$$

We consider the scattering cross section efficiency per unit length of the core-shell cylinder. The effective dipole moment of per unit length of the cylinder $\mathbf{P} = \varepsilon_h \alpha \mathbf{E}_0$, and the polarizability of the core-shell cylinder has the following expression,

$$\alpha = 2\pi\varepsilon_0 \left(\frac{D}{b^2} \right) b^2. \tag{18}$$

Similar to the case of finite particles, the scattering cross section σ_{sca} is defined for an incident beam of unit intensity scattered by a unit length of cylinder; therefore, we will have the scattering cross section from the polarizability by scattering theory within quasistatic approximation [42],

$$\sigma_{sca} = \frac{k^3}{8\varepsilon_0^2} |\alpha|^2, \tag{19}$$

and this leads to the following efficiency for scattering per unit cross section area of the incident filed as,

$$Q_{sca} = \frac{\sigma_{sca}}{2b} = \frac{2\pi^5 \varepsilon_h^{3/2} b^3}{\lambda^3} \left| \frac{D}{b^2} \right|^2. \tag{20}$$

To include the nonlinear effects, we assume the dielectric core as a Kerr-type medium, which has a field-dependent permittivity,

$$\varepsilon_c = \varepsilon_c^{(0)} + \chi^{(3)} |\mathbf{E}_c|^2, \tag{21}$$

where $\varepsilon_c^{(0)}$ is the linear part and $\chi^{(3)}$ is the third-order nonlinear coefficient.

In the composite system, for the electric field inside the core region $\mathbf{E}_c$ and outside field $\mathbf{E}_h$ in host medium, there is a relation,

$$\mathbf{E}_c = C\langle \mathbf{E}_h \rangle. \tag{22}$$

According to the 2D Clausius-Mossotti approximation, we have

$$\langle \mathbf{E}_h \rangle = \mathbf{E}_0 + \pi \langle \mathbf{P} \rangle, \tag{23}$$

where $\langle \mathbf{P} \rangle = N D \langle \mathbf{E}_h \rangle$. Here, N is the number of cylinders per unit volume. Considering the volume fraction of cylinder $f = \pi N b^2$ in 2D, one yields

$$\mathbf{E}_c = \frac{C}{(1 - f \cdot D/b^2)} \cdot \mathbf{E}_0. \tag{24}$$

Taking the square of modulus of Eq. (24), we have

$$|\mathbf{E}_0|^2 = |\mathbf{E}_c|^2 \cdot \left| \frac{1 - f \cdot D/b^2}{C} \right|^2. \tag{25}$$

Note that coefficients C and D are field dependent if we introduce the nonlinear Kerr type core, as shown in Eq. (21). Therefore, Eq. (25) indicates the nonlinear relation between external field and local field inside the core region, resulting in the potential optical bistability in near field of the core-shell cylindrical composite. Besides that, scattering efficiency defined in Eq. (20) also shows a nonlinear spectrum if we detect the scattering signal in the far field. In what follows, we

will give some numerical calculations and discussions mainly based on these two equations.

III. NUMERICAL RESULTS AND DISCUSSION

We are now in a position to give some numerical results. For numerical calculations, we introduce the hydrodynamic model [25,43] to describe the nonlocal shell: $\varepsilon_s = \varepsilon_g - \omega_p^2/[\omega(\omega + i\Gamma) - \beta^2 k^2]$, where $\varepsilon_g = 5$ is the background permittivity of the metal relating to the interband transition, $\omega_p = 1.367 \times 10^{16}$ s^{-1} and $\Gamma = 2.733 \times 10^{13}$ s^{-1} are the plasma frequency and the damping constant, respectively. β indicates the pressure term of electron gas, which is proportional to the Fermi velocity. Similar to the work in Ref. [35], we introduce decay length of longitudinal plasmons into metal $\delta = (\beta/c)\lambda_p$ (where $\lambda_p = c/\omega_p$) as degree of nonlocality. The aspect ratio is defined as $\eta = a/b$, and the outer radius is fixed at $b = 20$ nm in order to make the quasistatic approximation valid. Other parameters are $\varepsilon_c^{(0)} = 2.2$, $\chi^{(3)} = 4.4 \times 10^{-20}$ m^2/V^2, and $\varepsilon_h = 1$. To begin, we first investigate the scattering property from a linear core-nonlocal shell cylinder. Figures 1(a) and 1(d) show its scattering efficiency spectra under nonlocal and local descriptions respectively. Within the interested spectrum regime, there are two resonant modes and one cloaking mode. The resonant modes correspond to the hybridizations of the surface plasmon resonances at two interfaces of core-shell cylinder [44], and the cloaking mode shows very small scattering efficiency value. When the aspect ratio decreases, the cloaking mode and one of resonant modes begin to degenerate at one wavelength, leading to a narrowband Fano-like curve [21,45,46]. This closely spaced interaction of the cloaking dip and the resonant peak act as coupled dark and bright scattering states [see insert of Fig. 2(b)]. Compared with the local case, nonlocality will result in the wavelengths of both resonant and cloaking modes blueshifted especially for very small η, which is shown in Fig. 2(a). According to hybridization theory, with present parameters, antibonding dipole mode (λ_{1-}) is more dominated by cylindrical sphere mode (λ_s), and the bonding dipole mode (λ_{1+}) is close to cylindrical cavity mode (λ_c). Therefore, decreasing the inner radius will promote the nonlocal effects on the surface plasmon at the inner interface, which associates with the cavity mode. This will lead to a dramatic blueshift of bonding dipole mode (λ_{1+}). As to the antibonding dipole mode (λ_{1+}), however, the blueshift is not as obvious as that of the bonding one because the nonlocal effect is not dominated on the surface plasmon at outer interface with larger radius.

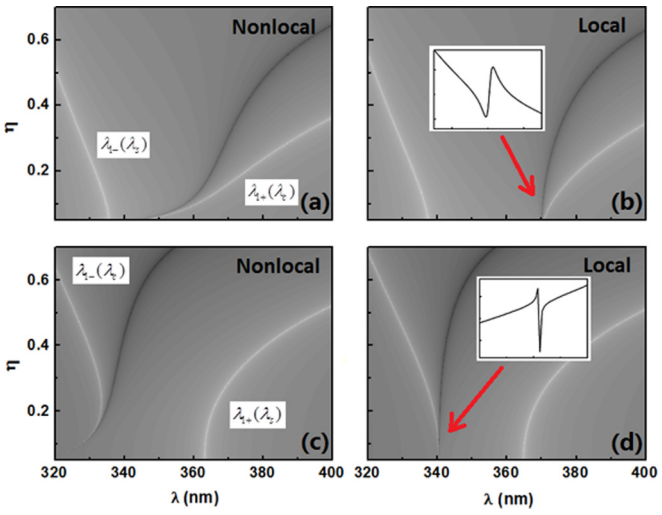

FIG. 2. $\log_{10}(Q_{sca})$ as function of incident wavelength and aspect ratio for core-shell cylinder [(a) and (b)] and core-shell sphere [(c) and (d)]. (a), (c) under the nonlocal descriptions; (b), (d) corresponding local cases. White and black lines in each panel show the minimal and maximal values, respectively, denoting different modes. The inserts in (b) and (d) show the results with $\eta = 0.05$.

The previous paper [45] indicated two different Fano-shape (S shape and Z shape) curves in the scattering spectra of core-shell type cylinder and sphere, respectively, in the local cases [see Figs. 2(b) and 2(d)]. However, this paper did not tell why that would happen. To illustrate the physics behind this, we plot the scattering spectra of the spherical case as well in both local and nonlocal descriptions in Figs. 2(c) and 2(d). In the $\eta \to 0$ limit and under local description, the cavity and cloaking modes have the same condition, i.e., $\varepsilon_c + \varepsilon_s = 0$ for the core-shell cylinder and $\varepsilon_c + 2\varepsilon_s = 0$ for the core-shell sphere. That means these Fano curves always go with cavity modes. Unlike the cylinder, the antibonding mode in the spherical core-shell case is dominated by cavity mode. Consequently, the Fano curve appears at the wavelength of antibonding mode on the left side and has a different Z-shape profile compared with cylinder [see Fig. 2(d)]. Moreover, the blueshift of resonant wavelength is more obvious on the antibonding mode. In fact, by choosing appropriate host and core media, the Fano shapes in both cylindrical and spherical core-shell cases are tunable. For simplicity, we clarify this in the local case and under the nondissipation limit. The Drude model for the shell is simplified as $\varepsilon_s = \varepsilon_g - \omega_p^2/\omega^2$. Equations $\varepsilon_s + \varepsilon_h = 0$ and $\varepsilon_s + 2\varepsilon_h = 0$ determine the sphere modes of cylindrical and spherical cases, respectively. Therefore, the resonant frequencies of sphere and cavity modes for each case can be written as

$$\omega_c^2 = \frac{\omega_p^2}{\varepsilon_c + \varepsilon_g}, \quad \omega_s^2 = \frac{\omega_p^2}{\varepsilon_h + \varepsilon_g} \quad \text{(for cylinder)} \tag{26}$$

$$\omega_c^2 = \frac{\omega_p^2}{\varepsilon_c/2 + \varepsilon_g}, \quad \omega_s^2 = \frac{\omega_p^2}{2\varepsilon_h + \varepsilon_g} \quad \text{(for sphere).} \tag{27}$$

Thus, one gains the following relations,

$$\begin{array}{lll} \omega_c > \omega_s & (\lambda_c < \lambda_s) & (\varepsilon_c < \varepsilon_h) \\ \omega_c < \omega_s & (\lambda_c > \lambda_s) & (\varepsilon_c > \varepsilon_h) \end{array} \quad \text{(for cylinder)} \tag{28}$$

and

$$\begin{array}{lll} \omega_c > \omega_s & (\lambda_c < \lambda_s) & (\varepsilon_c < 4\varepsilon_h) \\ \omega_c < \omega_s & (\lambda_c > \lambda_s) & (\varepsilon_c > 4\varepsilon_h) \end{array} \quad \text{(for sphere).} \tag{29}$$

The inequalities above indicate the positions of cavity and sphere modes on spectra under different conditions. In the calculations, we employ $\varepsilon_c = 2.2$ and $\varepsilon_h = 1$ for core and host media. Consequently, there is $\lambda_c > \lambda_s$ in scattering spectra of the core-shell cylinder and $\lambda_c < \lambda_s$ in that of the spherical case. This result demonstrates the different Fano-shape curves in Fig. 2. In the meantime, Eqs. (28) and (29) show that it

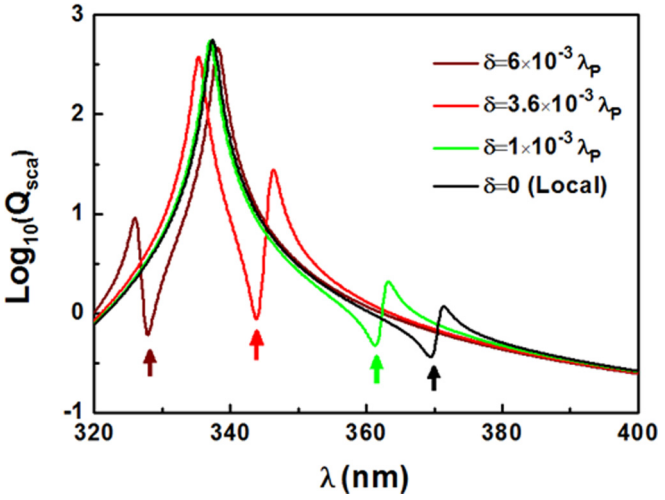

FIG. 3. Scattering efficiency spectra with different degrees of nonlocality.

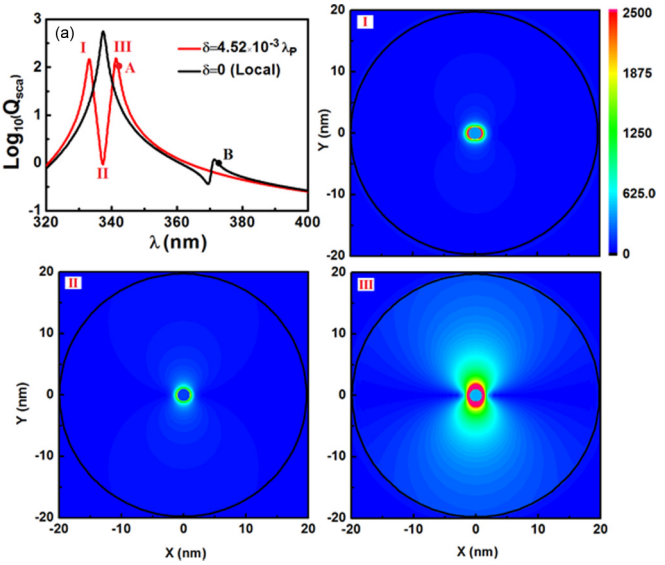

FIG. 4. (a) Scattering efficiency spectra with $\delta = 4.52 \times 10^{-3}\lambda_p$ and $\delta = 0$. I–III illustrate near-field $|\mathbf{E}|$ at corresponding points in (a).

is possible to rebuild the Fano shapes by choosing different physical parameters for core and host media.

From the discussion above, we could conclude that on one hand Fano resonance is determined by the cavity mode of the core-shell structure and on the other hand due to the nonlocal nature of the surface plasmon at the inner interface with very small radius, cavity mode is more sensitive to nonlocal effects. Therefore, it is possible to achieve tunable Fano resonances based on nonlocality. With different degrees of nonlocality, we plot the scattering efficiency spectra at a fixed aspect ratio $\eta = 0.05$ in Fig. 3. It shows that Fano curves vary dramatically with the degree of nonlocality. Increasing the degree of nonlocality will give more obvious blueshifted Fano resonances (see the Fano dips in Fig. 3). In addition, it is found that if δ reaches $6 \times 10^{-3}\lambda_p$, the Fano curve will change from an S shape into a Z shape. Different from the method of choosing different core and host media in the previous part, this kind of Fano-shape changing depends on the nonlocality of the metallic shell. Note that the Fano resonance would slightly vary with the aspect ratio in the local case; however, it could not achieve the transformation from S-shape Fano curve to a Z-shape one. Therefore, besides the variation of aspect ratio or dielectric materials, nonlocality would give a new freedom to adjust the Fano resonance in the core-shell type nanocylinder.

To one's interest, we use $\delta = 4.52 \times 10^{-3}\lambda_p$ as degree of nonlocality, in which case the cloaking dip lays in the right middle of two resonant peaks shown in Fig. 4(a). Unlike the conventional Fano resonance, which arises from the interference between a broadband background (nonresonant) scattering process and a sharp resonant state [see the local case in Fig. 4(a)], this non-Fano profile results more from the direct destruction of two resonant scattering states from the same scattering channel and forms a so-called scattering dark state [47]. Note that it still includes the background state here; therefore, the dip of the scattering dark state is not completely zero. Nevertheless, this curve profile is essentially different from the Fano resonance. We find that although the scattering efficiencies at position (I) and (III) are the same, their near-field distributions are dramatically different, as shown in Fig. 4. In details, near-field enhancement at inner interface in (III) is much larger than that in (I) due to the fact that resonant peak (III) is associated with the cavity mode. Besides that, the polarization direction of induced dipole fields are opposite in these two cases. As to (II), it is more like a monopole type for which the near field is uniformly distributed around the inner surface. Moreover, (III) reveals very high electric field intensity in the core region compared with others, which can be further employed to enhance the nonlinear optical response when using nonlinear core materials.

In what follows, we consider the nonlinear case in which Kerr-type nonlinear medium is used as core material whose permittivity has a field-intensity dependent dielectric function shown in Eq. (21). As mentioned before, near-field intensity in core medium is higher at bonding mode than others thus can promote the nonlinear response. On the other hand, to achieve optical bistability, physical parameters have to satisfy some specific conditions [16,48]. Within our parameter space, it is found that only the bonding mode has the possibility of showing optical bistability here. Figure 5(a) illustrates bistable $\mathbf{E_c}$ as the function of incident wavelength at different incident field intensities $\mathbf{E_0}$ for bonding resonant peak by solving the nonlinear Eq. (25). It is shown that the bistability of near field gets broader for increased input field intensity. Therefore, the proposed core-shell cylinder can realize a nonlinear nanoswitch device, whose switching wavelength is tunable with realistic incident field intensity. In addition, field intensity inside the nonlinear core can reach up to 1000 times the large value than the incident field intensity $\mathbf{E_0}$. Compared to the local case in Fig. 5(b), it has broader bistability region and lower switching wavelength at a same incident field intensity. Besides that, induced near-field intensity inside the core $\mathbf{E_c}$ is higher under the nonlocal description. That means nonlocality could further enhance the nonlinear response in the bonding modes. It is well known that nonlocality was generally found to reduce the near-field enhancement and far-field scattering of the nanostructures. In the present model, only the resonant

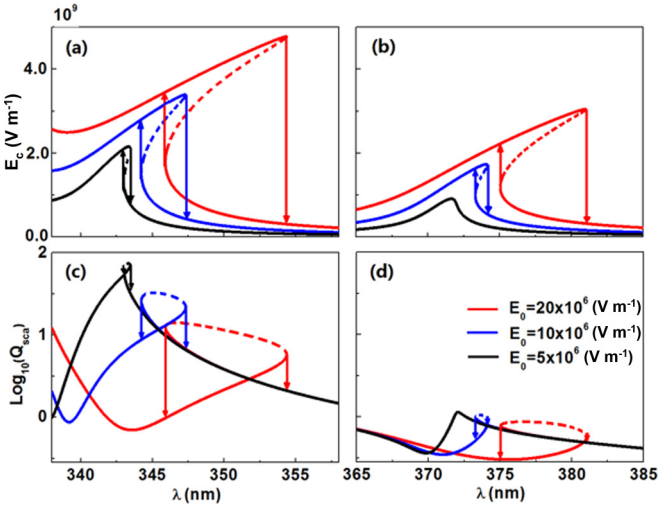

FIG. 5. Dependence of the electric field intensity $\mathbf{E_c}$ inside the core region on the incident wavelength at different $\mathbf{E_0}$ in nonlocal (a) and local (b) cases: $\mathbf{E_0} = 20 \times 10^6$ V m^{-1} (red), $\mathbf{E_0} = 10 \times 10^6$ V m^{-1} (blue), and $\mathbf{E_0} = 5 \times 10^6$ V m^{-1} (black). (c), (d) Scattering response versus wavelength at different $\mathbf{E_0}$ in nonlocal and local cases, respectively.

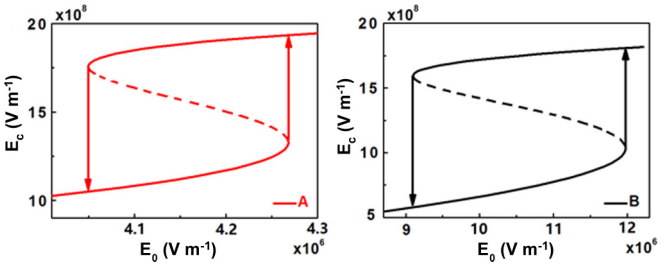

FIG. 6. Dependence of the electric field intensity $\mathbf{E_c}$ on external incident field $\mathbf{E_0}$ at (a) $\lambda = 343.1$ nm and (b) $\lambda = 373.8$ nm, respectively, which is denoted with A and B in Fig. 4(a).

peak of antibonding mode is reduced by nonlocality, and the bonding mode is, however, boosted by nonlocality. Nonlocality in the noble materials such as gold or silver is essentially a surface effect [43], which can modify the dielectric response at the surface, hence leading to the resonant wavelength shifted. Note that scattering spectra peak in Fig. 4(a) III is the result of constrictive interference of resonant bonding mode and off-resonant broadband antibonding mode. Once the resonant wavelength moves close to the high value antibonding resonant peak, the increased part from the broadband off-resonant antibonding mode will contribute to the rapid increased bonding mode peak III. Therefore, strong Fano coupling between these two resonant modes, as well as nonlocality together contribute to the prompted resonant peak III. For the antibonding peak I, nonlocal effects merely result in the conventional reduced resonant peak compared to the local case.

Next, the dependence of the far-field scattering property of this nonlocal core-shell cylinder is investigated as well. By substituting Eq. (25) into the field intensity dependent scattering efficiency in Eq. (20), one yields the nonlinear scattering spectra in Figs. 5(c) and 5(d). It should be noted that, although the nonlinear equation between $\mathbf{E_c}$ and $\mathbf{E_0}$ is derived in the composite system, the assumed volume ratio is quite small; therefore, the obtained scattering spectra are valid for a single core-shell cylinder in the host medium. Unlike the bistable near-field spectra, the scattering efficiency shows hysteresis loops in its spectra, which implies that multiple states do exist for the nonlinear core-shell cylinder, corresponding to different incident wavelengths. The nonlinear process in far-field spectra shows a more complicated variation in scattering signal than that in near-field spectra. As a matter of fact, these diffident states indicate quite different physical properties that the nanocylinder possesses. In view of possible technological applications, this finding is expected to be very useful. In addition, Fig. 5(c) reveals that maxima of scattering efficiency is decreased with the increase of incident field intensity, which shows opposite behavior compared to the near-field intensity in core region. This indicates different energy storage states inside the core-shell cylinder when the incident power is increasing. Similarly, once we neglect the nonlocality, the scattering efficiency will decrease, and the nonlinear property becomes weaker.

In the end, Figs. 6(a) and 6(b) show the hysteresis response of the proposed nonlinear core-shell cylinder as a function of the incident field intensity under nonlocal and local descriptions, respectively. Note that optical bistability occurs when the physical parameters satisfy some specific conditions [16,48]. As a matter of fact, we could not achieve optical bistability within present parameters when $\lambda < \sim 341$ nm in the nonlocal case (or $\lambda < \sim 372$ nm in the local case), as shown in Fig. 4(a). These critical points lay just near the maximal peak of the bonding resonance; therefore, the blueshifted bonding resonance arising from the nonlocality will lead to much border parameter space in spectra for achieving the optical bistability. Moreover, nonlocality will enhance the bonding resonant mode, hence contributing to its nonlinear response so that one might achieve a lower switching threshold intensity in the optical bistability of the near field. Figure 6 shows that the nonlocal switching threshold intensity is about one order of magnitude lower than that in the local case. Besides that, both cases could realize high intensity $\mathbf{E_c}$ inside the core region with lower incident field intensity $\mathbf{E_0}$ associated with nonlinear bistability.

IV. CONCLUSION

To conclude, we establish the nonlocal scattering theory for the nonlinear core-nonlocal shell cylinder and derive the nonlinear equations of near field and far field for the composite consisting of these cylinders in the quasistatic limit. Compared to the 3D spherical case, different types of Fano resonant shape exist in the scattering spectra of the core-shell cylinder when the aspect ratio is small. We demonstrate that Fano resonance always goes with the dominated cavity mode in the surface plasmon hybridization, and by appropriately choosing the core and host dielectric materials, it is possible to achieve different types of Fano curves artificially. In addition, nonlocal effects that could lead to the blueshift of the Fano peak will become more and more obvious when the inner radius of the core-shell structure decreases. This shifted Fano peak

is very sensitive to the degree of nonlocality, allowing the nonlocality-based tunable Fano curve. Increasing the degree of nonlocality would promote the maximal value of Fano resonant peak, which shows unconventional nonlocal effects. This Fano dip could reach to the scattering dark state once nonlocality reaches to a specific level. We found that nonlocality could enhance the nonlinear response of the core-shell structure not only in the near field but also in the far field at the Fano peak position because near field and scattering signal are both boosted by nonlocality. With the increasing power of the incident field, near-field intensity is enhanced in the spectra; however, far-field scattering efficiency shows opposite behavior. Finally, we study the optical bistability of the near field in the composite system, and again nonlocality is found to reduce the switching threshold of bistable curve, which suggests a nonlocality-enhanced optical bistability device.

It should be remarked that, quasistatic approximation used in theoretical part limits its extension in the case with large size. In this connection, we should introduce the self-consistent mean-field approximation in the framework of full wave Mie scattering theory [49,50] to deal with the electric field inside the Kerr medium. For a large size system, we will incorporate a full wave self-consistent mean-field approximation with extended nonlocal electromagnetic theory [30,43] to study the optical bistability beyond quasistatic approximation and analyze the contribution of high order scattering terms. Work along this line is in progress, and we shall report it elsewhere.

ACKNOWLEDGMENTS

The paper was supported by the National Natural Science Foundation of China (Grant No. 11374223), the National Basic Research Program (Grant No. 2012CB921501), the Qing Lan project, and the Project Funded by the Priority Academic Program Development of Jiangsu Higher Education Institutions.

[1] W. Cai and V. Shalaev, *Optical Metamaterials: Fundamentals and Applications* (Springer, New York, 2010).
[2] L. Kang, Y. H. Cui, S. F. Lan, S. P. Rodrigues, M. L. Brongersma, and W. S. Cai, Nature Commun. **5**, 4680 (2014).
[3] R. W. Boyd, *Nonlinear Optics, 3rd ed.* (Academic Press, Boston, 2008).
[4] M. Kauranen and A. V. Zayats, Nat. Photonics **6**, 737 (2012).
[5] A. V. Zayats, I. I. Smolyaninov, and A. A. Maradudin, Phys. Rep. **408**, 131 (2005).
[6] Y. Pu, R. Grange, C. L. Hsieh, and D. Psaltis, Phys. Rev. Lett. **104**, 207402 (2010).
[7] Y. Zhang, N. K. Grady, C. Ayala-Orozco, and N. J. Halas, Nano Lett. **11**, 5519 (2011).
[8] T. Hanke, J. Cesar, V. Knittel, A. Trugler, U. Hohenester, A. Leitenstorfer, and R. Bratschitsch, Nano Lett. **12**, 992 (2012).
[9] A. Mirzaei, A. E. Miroshnichenko, N. A. Zharova, and I. V. Shadrivov, J. Opt. Soc. Am. B **31**, 1595 (2014).
[10] D. A. Smirnova, I. V. Shadrivov, A. E. Miroshnichenko, A. I. Smirnov, and Y. S. Kivshar, Phys. Rev. B **90**, 035412 (2014).
[11] K. M. Leung, Phys. Rev. A **33**, 2461 (1986).
[12] R. Neuendorf, M. Quinten, and U. Kreibig, J. Chem. Phys. **104**, 6348 (1996).
[13] Y. R. Shen, Nature **299**, 779 (1982).
[14] L. Gao, L. P. Gu, and Z. Y. Li, Phys. Rev. E **68**, 066601 (2003).
[15] L. Gao, L. P. Gu, and Y. Y. Huang, Solid State Commun. **129**, 593 (2004).
[16] Y. Huang, A. E. Miroshnichenko, and L. Gao, Sci. Rep. **6**, 23354 (2016).
[17] R. Noskov, P. Belov, and Y. Kivshar, Sci. Rep. **2**, 873 (2012).
[18] R. E. Noskov, P. A. Belov, and Y. S. Kivshar, Phys. Rev. Lett. **108**, 093901 (2012).
[19] R. E. Noskov, A. E. Krasnok, and Y. S. Kivshar, New J. Phys. **14**, 093005 (2012).
[20] J. Butet and O. J. F. Martin, Plasmonics **10**, 203 (2015).
[21] C. Argyropoulos, P. Y. Chen, F. Monticone, G. D'Aguanno, and A. Alu, Phys. Rev. Lett. **108**, 263905 (2012).
[22] C. Argyropoulos, C. Ciraci, and D. R. Smith, Appl. Phys. Lett. **104**, 063108 (2014).
[23] J. B. Pendry, A. Aubry, D. R. Smith, and S. A. Maier, Science **337**, 549 (2012).
[24] R. Ruppin, Phys. Rev. Lett. **31**, 1434 (1973).
[25] C. Ciraci, R. T. Hill, J. J. Mock, Y. Urzhumov, A. I. Fernandez-Dominguez, S. A. Maier, J. B. Pendry, A. Chilkoti, and D. R. Smith, Science **337**, 1072 (2012).
[26] J. M. McMahon, S. K. Gray, and G. C. Schatz, Phys. Rev. Lett. **103**, 097403 (2009).
[27] C. David and F. J. G. de Abajo, J. Phys. Chem. C **115**, 19470 (2011).
[28] R. Esteban, A. G. Borisov, P. Nordlander, and J. Aizpurua, Nat. Commun. **3**, 825 (2012).
[29] A. Wiener, A. I. Fernandez-Dominguez, A. P. Horsfield, J. B. Pendry, and S. A. Maier, Nano Lett. **12**, 3308 (2012).
[30] Y. Huang and L. Gao, J. Phys. Chem. C **117**, 19203 (2013).
[31] Y. Luo, A. I. Fernandez-Dominguez, A. Wiener, S. A. Maier, and J. B. Pendry, Phys. Rev. Lett. **111**, 093901 (2013).
[32] T. V. Teperik, P. Nordlander, J. Aizpurua, and A. G. Borisov, Phys. Rev. Lett. **110**, 263901 (2013).
[33] N. A. Mortensen, S. Raza, M. Wubs, T. Søndergaard, and S. I. Bozhevolnyi, Nature Commun. **5**, 3809 (2014).
[34] Y. Huang, J. J. Xiao, and L. Gao, Opt. Express **23**, 8818 (2015).
[35] A. I. Fernandez-Dominguez, A. Wiener, F. J. Garcia-Vidal, S. A. Maier, and J. B. Pendry, Phys. Rev. Lett. **108**, 106802 (2012).
[36] D. C. Marinica, A. K. Kazansky, P. Nordlander, J. Aizpurua, and A. G. Borisov, Nano Lett. **12**, 1333 (2012).
[37] G. Hajisalem, M. S. Nezami, and R. Gordon, Nano Lett. **14**, 6651 (2014).
[38] C. Ciraci, M. Scalora, and D. R. Smith, Phys. Rev. B **91**, 205403 (2015).
[39] B. B. Dasgupta and R. Fuchs, Phys. Rev. B **24**, 554 (1981).
[40] F. J. G. de Abajo, J. Phys. Chem. C **112**, 17983 (2008).
[41] R. Rojas, F. Claro, and R. Fuchs, Phys. Rev. B **37**, 6799 (1988).

[42] M. Kerker, *The Scattering of Light and Other Electromagnetic Radiation* (Academic Press, New York, 1969).
[43] Y. Huang and L. Gao, J. Phys. Chem. C **118**, 30170 (2014).
[44] E. Prodan, C. Radloff, N. J. Halas, and P. Nordlander, Science **302**, 419 (2003).
[45] H. L. Chen and L. Gao, Opt. Express **21**, 23619 (2013).
[46] A. E. Miroshnichenko, S. Flach, and Y. S. Kivshar, Rev. Mod. Phys. **82**, 2257 (2010).
[47] C. W. Hsu, B. G. DeLacy, S. G. Johnson, J. D. Joannopoulos, and M. Soljacic, Nano Lett. **14**, 2783 (2014).
[48] D. J. Bergman, O. Levy, and D. Stroud, Phys. Rev. B **49**, 129 (1994).
[49] H. L. Chen, D. L. Gao, and L. Gao, Opt. Express **24**, 5334 (2016).
[50] H. L. Chen, Y. M. Zhang, B. L. Zhang, and L. Gao, Sci. Rep. **6**, 21741 (2016).